

FORCED VIBRATIONS OF A BEAM WITH ONE-SIDED AMPLITUDE CONSTRAINT: THEORY AND EXPERIMENT†

S. W. SHAW

*Department of Mechanical Engineering, Michigan State University, East Lansing
Michigan 48824, U.S.A.*

(Received 4 October 1983, and in revised form 15 May 1984)

An elastic beam with one-sided amplitude constraint subjected to periodic excitation is considered. Experimental results are obtained and compared with results given by a theoretical model based on a single mode analysis of the beam following the work of Moon and Shaw [1]. This model has been studied in some detail by the author in previous works [2–4], it is a single degree of freedom oscillator with periodic excitation and a piecewise linear restoring force. This single mode model is shown to provide good overall qualitative information about the actual physical system. It predicts the multiple subharmonic resonances, period doublings, and some chaotic regimes found experimentally.

1. INTRODUCTION

The motion of a beam subjected to amplitude constraints provides useful information about the behavior of mechanical systems and linkages with “play” or looseness. The response of such systems due to random excitation has been considered by Davies [5] and Wood and Byrne [6, 7]. Periodic forcing of these systems has been considered by Jones and Muszynska [8], Mariamy *et al.* [9], and Watanabe [10]. Single degree of freedom models of such systems have also received considerable attention (see the publications by Shaw and Holmes [2–4], and the references cited therein).

Moon and Shaw [1] have performed experiments similar to those described here and the derivation of the single mode model described in that work is reviewed below. The Moon and Shaw [1] experimental results were shown for a few discrete sets of a parameter values which demonstrated some of the non-linear phenomena exhibited by the system. In contrast, this work describes results from a more systematic variation of parameters. In particular, frequency response curves are obtained and compared with digital simulations of the single mode model. Also, two values for the stiffness ratio between constrained and free motions are considered. This ratio is altered by attaching a concentrated mass to the free end of the beam. Some of the effects of increasing this stiffness ratio have been previously predicted analytically but were not investigated experimentally [1]. As for digital simulations, Moon and Shaw [1] showed results for a single set of parameter values at which the experiment and the simulation showed a similar chaotic structure. Again, in the current article wide ranges of parameter values are used to compare results from experiments with those from the digital simulations of the single mode model. The theoretical results found by Shaw and Holmes [2] are also checked against the experimental results where appropriate.

The aim of this work was to obtain a qualitative comparison between a complicated non-linear system, the forced beam with constraints, and a simplified model of that system.

† Work done while a graduate student in the Department of Theoretical and Applied Mechanics, Cornell University, Ithaca, New York 14853, U.S.A.

Such a comparison was carried out over a wide range of parameter values and a variety of non-linear behaviors are shown to be captured by the simple model. As well as predicting the chaotic motions as described in reference [1], the model also predicts subharmonic resonances, period doublings, and the specific parameter regions where chaos may be expected to be found to occur as well.

2. DESCRIPTION OF THE EXPERIMENTAL MODEL

The experimental system consists of a beam clamped at one end, with non-linear boundary conditions at the other end. The unclamped end is effectively pinned for tip displacements greater than some value and is free otherwise (see Figure 1). This system

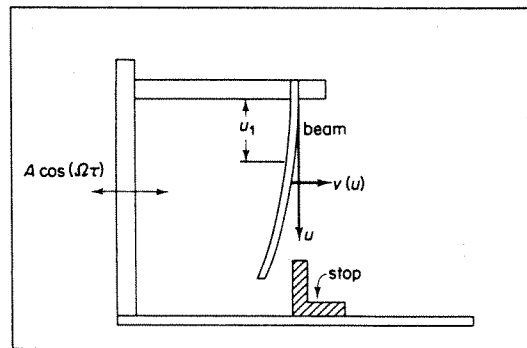


Figure 1. The experimental apparatus.

and the following derivation of the equation of motion is similar to that described by Moon and Shaw [1]. Here the investigation is concentrated on the case where the tip amplitude constraint is positioned centrally: i.e., at the equilibrium point of the free beam. Of course, a beam has a very large number of degrees of freedom. Therefore modal analysis is used to reduce the governing partial differential equation to a single second-order ordinary differential equation. The equation of the beam relative to the moving support is

$$(EIv'')'' = -m(\ddot{v} + \ddot{A}), \quad (1)$$

where v is the lateral displacement of the beam relative to its equilibrium position, A is the displacement of the clamped end, m is the mass per unit length, EI is the bending stiffness of the beam, $(\)'$ refers to a derivative with respect to u , the distance along the beam, and $(\)^\circ$ refers to a time derivative, $d/d\tau$. For a given set of boundary conditions, $v(u, \tau)$ may be written in terms of the modes of the beam $\{\phi_i(u)\}$. In this analysis the system is reduced to a single modal equation by taking

$$v(u, \tau) = a_i(\tau)\phi_i(u), \quad (2)$$

where $i = 1, 2$ depending on the boundary conditions. In equation (2), the mode shape $\phi_i(u)$ used will depend on whether or not the tip amplitude is constrained. This procedure will lead to a single second-order ordinary differential equation in the modal amplitude $a(\tau)$ with a piecewise linear restoring force (due to the different modal stiffnesses) and piecewise constant forcing amplitude and damping coefficient. With this model only the non-linear restoring force is dealt with and there is no attempt to account for the discontinuous nature of the damping or forcing amplitude. Moon and Shaw [1] did account for the jump in forcing amplitude with the change in mode, but used a Runge-

Kutta numerical integrator to analyze the resulting equation of motion. In contrast, in this work the digital simulations and theory described in reference [2] and reviewed below are compared with the experimental results with a view to obtaining a qualitative comparison.

The experimental apparatus is the same as that described in reference [1]. The beam and support shown in Figure 1 were excited by using an electromagnetic shaker. Strain gages at the base ($u \sim 0$) of the beam were used to measure the motion. This positioning of the gages allows for measurements of the strain at a particular point on the beam only. Several modes may contribute to that strain and thus it does not allow precise quantitative measurements to be done. However, qualitative measurements are possible since a periodic motion of the beam will certainly be reflected by a periodic strain measurement. Likewise chaotic behavior may be detected.

The strain-gage signal was put through an amplifying bridge circuit and then through an active filter. This filtered displacement signal was then differentiated in real time by using an electronic differentiation circuit. The strain-gage and its time derivative were then used to generate phase portraits and Poincaré maps [1]. The Poincaré maps of orbits were obtained by amplifying the oscilloscope intensity at one point on each cycle of the forcing signal, a modulation signal from the driving oscillator being used. At a particular phase of the forcing function the amplified signal would place a dot on the screen of the storage oscilloscope, thus generating a Poincaré map. Strain and strain-rate signals were also fed to a dual-channel digital oscilloscope and a portion of the data stored for analysis and for subsequent plotting of the time traces and phase portraits presented in this paper. For additional damping, shim steel was attached to both sides of the beam by using double-sided adhesive tape.

Two cases were considered. The first is as shown in Figure 1. In the second case a concentrated mass is attached to the free end of the beam, significantly increasing the stiffness ratio. As will be described in what follows, in both cases the governing modal equations were derived and system parameters calculated. Then these parameters were measured experimentally from free oscillation data. Experimental results were then compared to theory and digital simulations where possible.

The dimensions of the beam are as follows: length $L = 18.8$ cm; width $w = 9.5$ mm; thickness $h = 0.23$ mm. The tip amplitude constraint was placed at the origin ($v = 0$) in all of these experiments.

3. MODERATE STIFFNESS RATIO

3.1. THEORETICAL MODEL

For a moderate stiffness ratio the modes used are $\phi_1(u)$ when $v(L) < 0$, the fundamental mode for a clamped-free beam, and $\phi_2(u)$ when $v(L) = 0$, the fundamental mode for a clamped-pinned beam. One multiplies equation (1) by $\phi_i(u)$ and integrates from 0 to L , using equation (2) and $EI = \text{constant}$, to obtain

$$EI a_i \int_0^L \phi_i(u) \phi_i'''(u) du = -m \left(\ddot{a}_i \int_0^L \phi_i^2(u) du + \ddot{A} \int_0^L \phi_i(u) du \right). \quad (3)$$

From the book by Blevins [11] one has

$$\int_0^L \phi_i(u) \phi_i'''(u) du = \beta_i^4 \int_0^L \phi_i^2(u) du, \quad \int_0^L \phi_i^2(u) du = L, \quad (4)$$

$$\int_0^L \phi_i(u) du = I_i, \quad i = \begin{cases} 1, & v(L) < 0 \\ 2, & v(L) = 0 \end{cases},$$

where

$$I_1 = 2\sigma_1/\beta_1, \quad I_2 = [(\sigma_2^2 + 1)^{1/2} - (\sigma_2^2 - 1)^{1/2} + 2\sigma_2]/\beta_2, \quad \sigma_1 = 0.734, \quad \sigma_2 = 1.001, \\ \beta_1 = 1.875/L, \text{ and } \beta_2 = 3.927/L. \text{ Using equations (4) in equation (3) gives}$$

$$\ddot{a}_i + (EI/m)\beta_i^4 a_i = -(I_i/L)\ddot{A}, \quad i = 1, 2. \quad (5)$$

To make the modal amplitude continuous one considers the displacement at a particular point on the beam, $u = u_1 = 0.32L$, where $\phi_1(u_1) = 1$ and $\phi_2(u_1) = 1.48$, and defines

$$a(\tau) = \begin{cases} a_1(\tau), & a < 0 \\ a_2(\tau)\phi_2(u_1) = 1.48a_2(\tau), & a > 0 \end{cases} \quad (6)$$

Upon using this expression equation (5) becomes the desired single equation

$$\ddot{a} + \frac{EI}{m} \begin{pmatrix} \beta_1^4, & a < 0 \\ \beta_2^4, & a > 0 \end{pmatrix} a = \begin{cases} -I_1, & a < 0 \\ -I_2, & a > 0 \end{cases} \frac{1}{L} \ddot{A}. \quad (7)$$

This equation has the required feature of a piecewise linear restoring force. However, one also can note that there is a jump in the forcing amplitude. For the modes being considered the ratio $(\beta_2/\beta_1)^4 = 19.2$ while $(I_2/I_1) = 1.11$. Thus, the largest non-linearity is in the restoring force. Linear damping is added and one considers harmonic excitation $A(\tau) = A \cos(\Omega\tau)$ to obtain

$$\ddot{a} + 2\gamma\dot{a} + \frac{EI}{m} \begin{pmatrix} \beta_1^4, & a < 0 \\ \beta_2^4, & a > 0 \end{pmatrix} a = \begin{cases} I_1, & a < 0 \\ I_2, & a > 0 \end{cases} \frac{A\Omega^2}{L} \cos(\Omega\tau), \quad (8)$$

which is exactly the model studied in reference [2] except for the small jump in forcing amplitude. It should be noted that any non-linear damping features, including possible jumps due to the bi-modal expansion, are not included in equation (8). Also it should be noted that the second mode in the clamped-free configuration has a natural frequency substantially higher than that for $\phi_2(u)$, the first clamped-pinned mode. This fact, along with the extra damping added to the system, lends credence to the validity of the single-mode analysis.

Equation (8) has a piecewise linear restoring force whose slope changes at $a = 0$. Consideration of the unforced, undamped ($A = 0$, $\gamma = 0$) system shows that the natural frequency of this system is *amplitude independent*. This is not typical of a non-linear system and is due to the nature of the non-linearity. The undamped natural frequencies for $a > 0$ and $a < 0$ are defined as $\omega_+^2 = (EI/m)\beta_2^4$ and $\omega_-^2 = (EI/m)\beta_1^4$, respectively. One can easily compute the system's undamped natural frequency to be

$$\omega_n = 2\omega_+\omega_-/(\omega_+ + \omega_-), \quad (9)$$

using the known excursion times in $a > 0$ and $a < 0$. With the jump in forcing amplitude at $a = 0$ ignored by using an average \bar{I} equation (8) may be rewritten as

$$\ddot{a} + 2\gamma\dot{a} + \begin{cases} \omega_+^2, & a > 0 \\ \omega_-^2, & a < 0 \end{cases} a = \bar{I} \frac{A\Omega^2}{L} \cos(\Omega\tau). \quad (10)$$

By rescaling time and displacement by introducing the non-dimensional time $t = \omega_- \tau$ and displacement $x = a(L/\bar{I}A)(\omega_-/\Omega)^2$, respectively, the non-dimensional equation of motion is obtained,

$$\ddot{x} + 2\alpha\dot{x} + \begin{cases} \tilde{\omega}^2, & x \geq 0 \\ 1, & x < 0 \end{cases} x = \cos(\omega t), \quad (11)$$

where $\alpha = \gamma/\omega_-$, $\tilde{\omega} = \omega_+/\omega_-$, and $\omega = \Omega/\omega_-$. Note that the forcing amplitude has been scaled out; this is desirable in the special case considered here since the system's natural frequency is amplitude independent. The scaling behavior of this system (with the constraint at the unforced equilibrium position) is like that of a linear system in that changes in forcing amplitude simply change the size of the orbits *proportionally* (see references [2, 3] for more details). In more general non-linear systems a rescaling which leaves a forcing amplitude parameter is more appropriate since it gives one a "dial" with which actual phenomena, not just orbit size, may be changed. In contrast, the model considered here predicts behavior independent of the forcing amplitude and the experiments discussed below bear this out. A simple physical model whose motions are governed by equation (11) is shown in Figure 2.

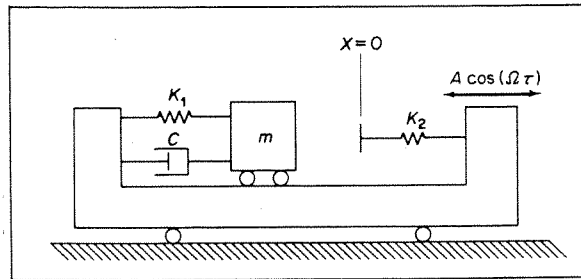


Figure 2. The single mode model.

Digital simulations of such a model were performed as follows. The governing linear equations for $x > 0$ and for $x < 0$ given by equation (11) are solved explicitly. These expressions are matched in time and velocity along $x = 0$ to obtain a complete solution. This matching is straightforward in principle but does require the solution of a transcendental equation for the $x = 0$ crossing time (see references [2-4] for more details on this simulation).

The stiffness ratio in this model is $(\beta_2/\beta)^4 = 19.2$. Equation (8) shows that motions of mechanical systems with amplitude constraints naturally give rise to equations of motion containing piecewise linear terms. The actual physical data is now considered.

3.2. EXPERIMENTAL RESULTS—COMPARISON WITH THEORY

Figure 3(a) shows free oscillations of the beam without the stop. From this data the frequency of the clamped-free mode was measured to be $\Omega_- = 28.2$ rad/s. Figure 3(b) shows free oscillations of the beam with the stop in place. The system's natural frequency was determined to be $\Omega_n = 43.6$ rad/s from this data and was nearly amplitude independent as expected. Also from these data an equivalent linear damping coefficient of $\alpha = 0.083$ was computed by using the log decrement method. Using the above two frequencies Ω_n and Ω_- one can compute the clamped-pinned frequency via the expression analogous to equation (9) which includes damping:

$$\Omega_n = 2\Omega_+\Omega_-/(\Omega_+ + \Omega_-), \quad \text{where } \Omega_+^2 = \omega_+^2 - \gamma^2, \quad \Omega_-^2 = \omega_-^2 - \gamma^2. \quad (12)$$

It is determined that $\Omega_+ = 96.1$ rad/s. These parameters are fixed for this set of experiments as is the stop location which is placed at the equilibrium position of the beam. The forcing frequency and amplitude were varied.

For these experimental parameter values the non-dimensional stiffness ratio is determined to be $\tilde{\omega}^2 = 11.6$. The experimental value is significantly lower than that predicted

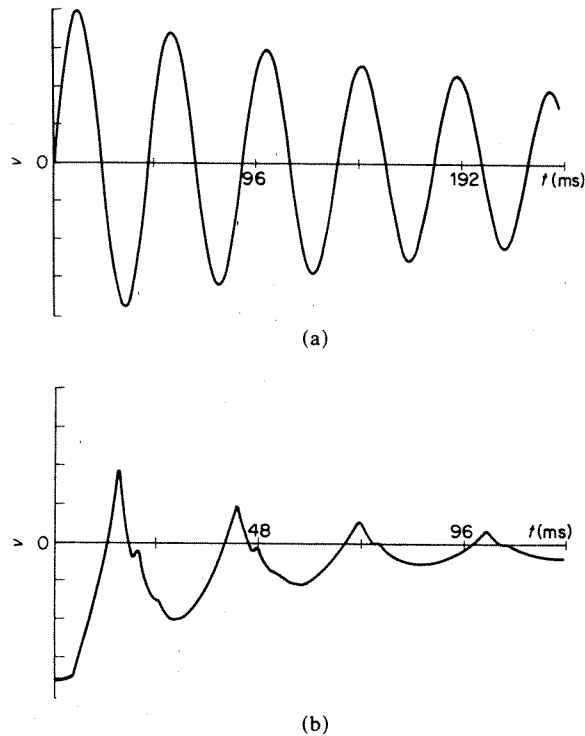


Figure 3. Free oscillations (strain versus time) $\omega^2 = 11.6$. (a) Without the stop; (b) with the stop.

above. This is most likely due to the added mass of the two strips placed on the beam for damping. These strips add significant mass but not much stiffness since they do not extend up to the base of the beam $u = 0$.

The theoretical model in reference [2] predicts that a period doubling bifurcation should occur at a set of critical parameter values given by (under an assumption regarding the times of flight in $a \geq 0$)

$$\alpha/\omega = (1/2\pi) \ln [(\hat{\Omega}s^2 - c^2) - \sqrt{(\hat{\Omega}s^2 - c^2)^2 - 1}], \quad (13)$$

where $s = \sin(\pi\Omega_n/\Omega)$, $c = \cos(\pi\Omega_n/\Omega)$, and $\hat{\Omega} = \frac{1}{2}\{(\Omega_+^2 + \Omega_-^2)/(\Omega_+ \Omega_-)\}$. This bifurcation changes the stability of a simple single impact periodic motion with frequency equal to that of the forcing. As the orbit becomes unstable a new stable motion appears containing two impacts and having frequency half that of the forcing. By solving equation (13) for the parameter values determined above, a critical value of forcing frequency is obtained: $\omega_{cr} = 2.28$ ($\Omega_{cr} = 64.3$ rad/s). (Recall that Ω refers to actual frequency and ω to scaled frequency.) Figure 4 shows phase portraits from the experiment at $\Omega = 65.4$ rad/s ($\omega = 2.32$) and $\Omega = 68.1$ rad/s ($\omega = 2.41$) between which a period doubling has occurred. Here the single degree of freedom model predicts the period doubling bifurcation value to within experimental error. Digital simulations performed as described above show that the actual period doubling for the one degree of freedom model occurs at $\omega_{cr} = 2.37$, also close to the experimental value. The model performs extremely well in predicting this period doubling value. One can also note that the experimental period doubling value was found to be largely independent of the forcing amplitude. In fact there was less than a 2% difference in the experimental values of ω_{cr} over a range of peak-to-peak forcing amplitudes of 4 to 10 mm. The model predicts such independence. The effect of varying

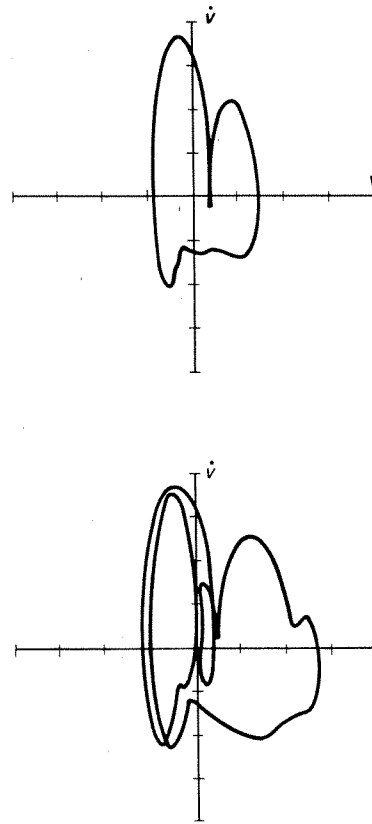


Figure 4. Phase portraits (strain rate versus strain) showing period doubling. (a) $\omega = 2.32$, period one single-impact motion; (b) $\omega = 2.41$, period two double-impact motion.

the constraint position was not investigated in this set of experiments (see reference [1] for studies of such effects).

This section is concluded by showing an orbit of period three at frequency $\Omega = 122$ rad/s ($\omega = 4.33$) and peak-to-peak forcing amplitude of 5 mm (see Figure 5). This orbit appears with increasing ω after the period-two orbit described above has developed. In fact, in reference [2] it is shown that as the forcing frequency is increased the period-two orbit

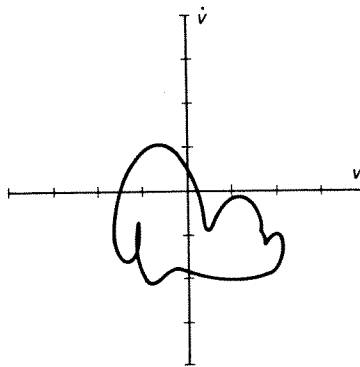


Figure 5. Phase portrait (strain rate versus strain) of a period three orbit.

should once again collapse onto the period-one orbit. In the experiment the period-two orbit does disappear near the point where the period-three orbit shown appears. Thus, coexistence of period-one and period-three orbits may be expected. However, a period-one orbit could not be located for certain, although very long transients were often encountered enroute to the period-three orbit. These transients may be due to the existence of horseshoes (see reference [2]) or due to the existence of a stable period-one orbit which has a small domain of attraction, in which case noise (small perturbations) in the system might prevent motions from approaching the orbit.

4. LARGE STIFFNESS RATIO

4.1. THEORETICAL MODEL

In this section results from experiments performed on a modified, large stiffness ratio, version of the system shown in Figure 1 are presented. The system is modified by adding a concentrated mass M (a brass cylinder of mass 7.6 grams) to the end of the beam, thus lowering the frequency of the clamped-free mode, ϕ_1 . The frequency of the clamped-pinned mode, ϕ_2 , is not changed because the mass (ideally) remains in contact with the stop during that part of the motion for which $v(L) = 0$. However, complications arise in this situation since the mass actually rebounds upon collision with the stop. A modal analysis is again used to predict analytically system parameter values.

In this case the pinned mode ϕ_2 is the same as before, but ϕ_1 must be approximated because of the mass loading at $u = L$. Using the method of assumed modes one writes (after reference [12], page 33)

$$\phi_1(u) = \frac{1}{2}[3(u/L)^2 - (u/L)^3]. \quad (14)$$

The modal stiffness and modal mass (see, for example, reference [13], p. 269) are given respectively by

$$K_1 = \int_0^L EI[\phi_1''(u)]^2 du \quad \text{and} \quad m_1 = \int_0^L m[\phi_1(u)]^2 du + M\phi_1^2(L), \quad (15)$$

where m is the mass per unit length of the beam. Here the density $\rho = 7700 \text{ kg/m}^3$ and modulus of elasticity $E = 2 \times 10^{11} \text{ N/m}^2$ for steel are used and $I = wh^3/12$. The results are $m = 1.68 \times 10^{-2} \text{ kg/m}$ and $I = 9.63 \times 10^{-3} \text{ mm}^4$. Using these quantities in equations (15) gives $\omega_1^2 = K_1/m_1 = 119 \cdot \text{rad}^2/\text{s}$, and $\omega_2^2 = \beta_2^4(EI/m) = 2.61 \times 10^4 \text{ rad}^2/\text{s}^2$ (from the previous section). The theoretical stiffness ratio is $(\omega_2/\omega_1)^2 = \bar{\omega}^2 = 218$, about a factor of ten higher than before. The experimentally determined stiffness ratio discussed below is again considerably smaller than this predicted value. The jump in forcing amplitude will also be larger in this case but again will be ignored since its effect on the motion is likewise reduced since the system will spend less time in the constrained configuration. Also, the magnitude of the jump in the forcing amplitude is less than the corresponding one in stiffness as was the case earlier.

4.2. EXPERIMENTAL RESULTS—COMPARISON WITH THEORY

Figure 6(a) shows free oscillations of this system without the stop. The natural frequency and damping coefficient are determined to be $\Omega_- = 14.4 \text{ rad/s}$ and $\alpha = 0.014$, respectively. Figure 6(b) shows free oscillations of the system with the stop. The damping is much larger here due to losses incurred at the (multiple) impact(s). The natural frequency here is determined to be $\Omega_n = 24.6 \text{ rad/s}$. The clamped-pinned frequency via equation (12) is determined to be $\Omega_+ = 86.4 \text{ rad/s}$. The experimentally determined stiffness ratio is therefore $\bar{\omega}^2 = 36.1$. Using a log decrement procedure to obtain an equivalent linear damping

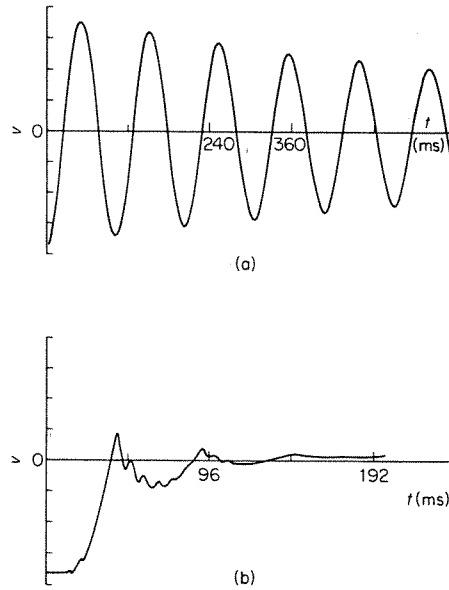


Figure 6. Free oscillations (strain versus time) $\omega^2 = 36.1$. (a) Without the stop; (b) with the stop.

constant yields $\alpha = 0.230$. The following experimental results will be compared with the digital simulations in which this damping coefficient was used.

Examination of Figure 6(b) motivates some comments. First, it should be noted that the large losses incurred at impact reduce the aforementioned complications due to the rebound of the mass. Also, it is obvious from the time trace shown that the frequency and damping parameters can be estimated only very roughly. For the present study, such estimates are adequate since one is primarily interested in the gross behavior as parameters change and not on precise measurements.

In the following frequency response curve the maximum tip displacement (i.e., $d = v(L)_{\max} = a(\tau)_{\max}$ since $\phi_1(L) = 1$) versus the forcing frequency on periodic motions is plotted. In order to compare the experimental data with results from the model it must be scaled appropriately. The non-dimensional displacement x is related to the modal amplitude a by $x = (L/\bar{I}A)(\omega_-/\Omega)^2 a$, where ω_-^2 represents the square of the unconstrained system's natural frequency, A is the forcing amplitude, Ω is the forcing frequency and $\Omega_-^2 (\approx \omega_-^2$ to order α^2) has been measured experimentally. In the experiment A was held fixed and Ω was varied. At each Ω value several cycles of the orbit were stored in the digital oscilloscope and the maximum strain signal was recorded. Several sample orbits were plotted by sending the data from the digital oscilloscope into a minicomputer which then plotted the data. The maximum tip displacement, d , was calculated by using a static calibration. The calibration constant was determined to be $c = 0.0427$ mm/mV from a least squares fit of the static tip displacement versus voltage data. As mentioned above, the strain signal includes components from many active modes, and hence the measured signal may not precisely represent the tip displacement during dynamic measurements. The calibration constant was used in the calculations, it being assumed that the signal from the fundamental mode would be the major contribution to the total signal. The non-dimensional tip displacement x is computed by using $d = Vc = a(\tau)_{\max}$ and $\bar{I} = L$, to obtain

$$x_{\max} = (\omega_-/\Omega)^2 (Vc/A) = (\Omega_-/\Omega)^2 (Vc/A). \quad (16)$$

A plot showing the experimental values of x_{\max} , the maximum displacement between impacts, versus the dimensionless frequency $\omega = (\Omega/\Omega_-)$ is shown in Figure 7(a). Note that there exist multiple resonances as predicted from the theory in reference [2], and that the resonance peaks are centred to the left of the even integers. This is expected since the "undamped" theory predicts peaks at the even integers and the large damping accounts for the leftward shift. The insets show time traces (x versus t) of typical orbits at selected frequencies. In Figure 7(b) results from the digital simulation are shown with

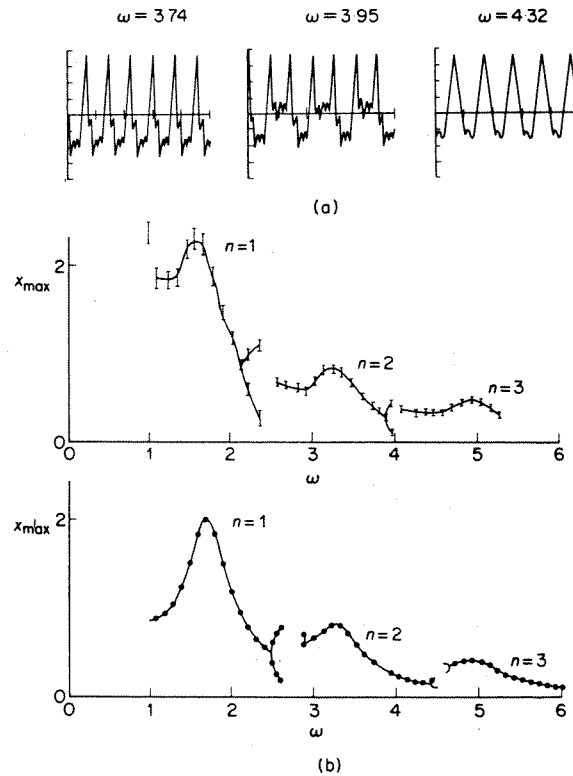


Figure 7. Frequency response curves, X_{\max} versus ω . (a) Experimental; (b) digital simulation.

$\tilde{\omega}^2 = 36.1$, $\alpha = 0.23$, and with ω varying. The plot shows the maximum displacement between impacts. Thus, where two branches are present for a given ω the motion is a double impact periodic orbit. Comparison with the experimental results shows that the qualitative features agree and also quantitative agreement is reasonable. Thompson [14] has shown similar resonance plots produced numerically for various $\tilde{\omega}$. Each subharmonic resonance, labeled by its period, n , in Figure 7 corresponds to a motion which repeats each $2\pi n/\omega$ in time and strikes the constraint once during that time. As plotted the resonance peaks decrease with increasing n ; this is due to the rescaling (equation (16)) and it should be noted that the physical displacements are large for all n observed. These resonances are *not* due to higher beam modes.

The error bars in Figure 7(a) are due mainly to an uncertainty in the forcing amplitude A . The base motion was measured by using a linear variable differential transducer and the peak-to-peak amplitude was held to $6 \text{ mm} \pm 0.3 \text{ mm}$, a 5% uncertainty. Thus the error is proportional to x , via equation (16).

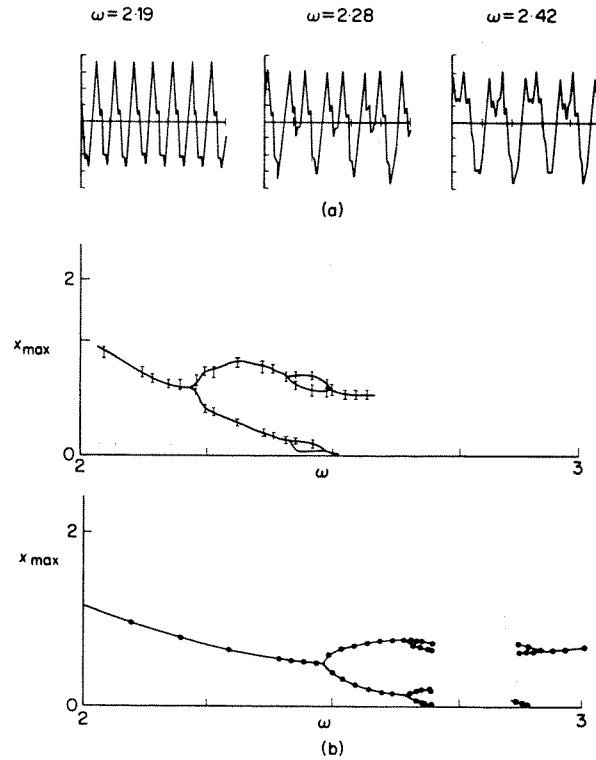


Figure 8. Frequency response between the $n = 1$ and $n = 2$ resonance peaks, x_{\max} versus ω . (a) Experimental; (b) digital simulation.

In Figure 8(a) a bifurcation diagram is shown for the region between the $n = 1$ and $n = 2$ resonances in greater detail in order to show how the transition from single impact period-one to single impact period-two motion occurs. This experimental data shows that the $n = 1$ orbit period doubles as predicted by the theoretical model (see Figure 8(b)). It then period doubles again to a period-four, four-impact orbit. This orbit then undergoes a (reverse) bifurcation and a transition to a single impact period-two motion. (Transitions occur when one of the maximum displacements between impacts goes to zero [2, 3].) The insets show time traces (x versus t) of typical orbits at selected frequencies in the sequence. No chaotic orbits were found experimentally in this band as were found in the model [2]. This is probably due to the large damping in the system. However, note the transitions described in references [2-4] for the case of large dissipation do occur in the physical system and do in fact change the nature of the orbits. Thus, as expected, degenerate orbits play an important role in the development of periodic orbits in these impacting systems.

Single impact period- n orbits were observed up to $n = 8$. Each of these resonance bands exhibited similar structures: a central peak between $\omega = 2n$ and $2n - 1$ and period doublings on each side of the peak. The bands between n and $n + 1$ single impact orbits were found to contain many periodic orbits, including evidence of period doubling sequences and other multiple impact periodic orbits as well as chaos. For example, between the $n = 5$ and $n = 6$ bands an apparently chaotic motion was observed and an experimental time T Poincaré map (see reference [15]) was obtained in which the displacement and velocity are plotted once per period of the forcing T . Thus a period- n subharmonic

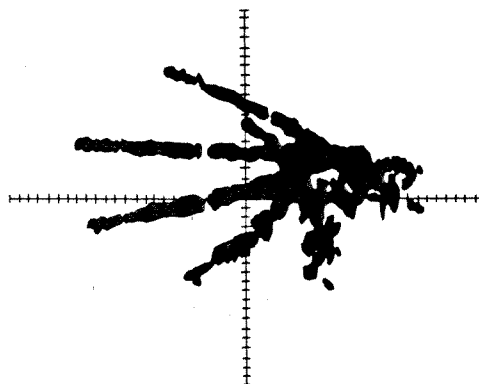


Figure 9. Poincaré map between the $n = 5$ and $n = 6$ resonance peaks, experimental.

appears as a set of n points in the Poincaré map. A photograph of a segment of the orbit is shown in Figure 9. There is evidence of some structure although the Cantor-sheet-like structure found in other "strange attractors" is not evident, probably due to the relatively large damping (see reference [15] for an example). However, the structure found here does match that shown by the digital simulation reasonably well. Parameters $\omega = 11$ and $\alpha = 0.23$ were used to obtain a time T Poincaré map for the model. For this simulation the "impact limit" was used where $\tilde{\omega} \rightarrow \infty$ and a simple reversal of velocity at $x = 0$ is used in place of the $x > 0$ excursion. This is reasonable for large $\tilde{\omega}$ as shown in reference [2]. Figure 10 shows the orbit. Thompson [14] showed similar numerical results in the $n = 4, 5$ band. The similar structure of the orbits indicates that a single degree of freedom model gives good qualitative results not only for periodic orbits but for apparently non-periodic orbits as well. Moon and Shaw [1] have made the same observation when comparing experiments and digital simulations.

The structure of the experimentally obtained frequency response curve (see Figure 7(a)) is remarkably similar to that obtained from the digital simulation of the single-mode

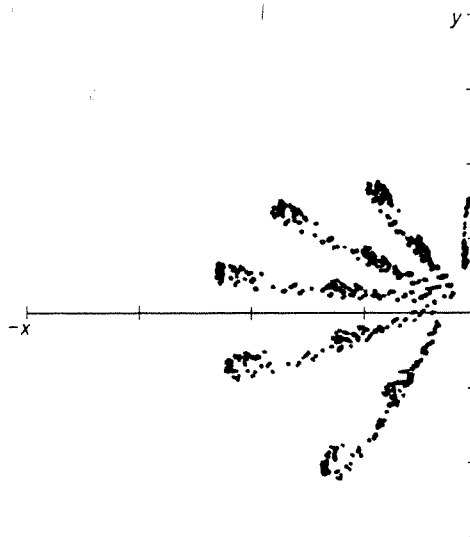


Figure 10. Poincaré map between the $n = 5$ and $n = 6$ resonance peaks, digital simulation.

model (see Figure 7(b)). The single impact periodic motions of the model can be found analytically [2] in the $\tilde{\omega} \rightarrow \infty$ limit, and the period doubling parameter values from these motions are given explicitly in that reference also. The chaotic motions found to occur between the resonance peaks seem to be possible only for sufficiently large values of $\tilde{\omega}$. This feature, roughly demonstrated here, has been predicted by Thompson [14] using digital simulations. Also, Moon and Shaw [1] reported that no chaotic-looking motions were observed for the case when no concentrated mass was attached to the beam (lower $\tilde{\omega}$) and the stop was centrally located. As shown here, systems in which the stop is so placed can indeed exhibit chaos if the stiffness ratio $\tilde{\omega}$ is large enough.

5. CONCLUSIONS AND DISCUSSION

- : An elastic beam with one-sided amplitude constraint and periodic external excitation was experimentally shown to exhibit non-linear behavior including subharmonic resonances, period doublings and chaos. This system was studied by using a simple single-mode model as in reference [1] and experimental results were compared with results obtained from that model. The resulting single degree of freedom oscillator has been studied in detail both theoretically [2-4] and numerically [2-4, 14]. These experiments complement those works.

Oscillating and impacting systems have many applications including impact print hammers [16], steam generator tubes [9, 17], machinery noise [6, 7], and moored marine vessels [14, 18]. The results in this paper demonstrate that a simple model provides useful information about the response of such systems when subjected to periodic forcing. It is encouraging that the influence of such extremely "hard" non-linearities is captured by such models and that reasonable quantitative information, as well as overall qualitative behavior, can be obtained from them. Response curves such as Figure 7 may be used in the design of mechanical systems; the large amplitudes of the subharmonic resonances and the possible long-period or chaotic motions between them may be avoided by appropriate parameter choices.

The apparently *random* response of many systems may in fact be *deterministic* if non-linearities are large. Experimental power spectra from chaotic motions [1, 19, 20] reflect the existence of unstable periodic motions and also contain a broad-band background. Mathematical models of chaos (in particular the Smale horseshoe [2, 21]) allow *any* amount of *any* period motion to exist in the spectrum and cannot currently predict the nature of these spectra in most systems. Simple one-dimensional maps undergo a well understood bifurcation sequence and in some special cases their spectra are well understood [22, 23]. However, in recent work in dynamical systems theory it has been verified that the bifurcations to subharmonic and to transient and steady state chaotic motions in more complex systems are not the same as those in the one-dimensional maps and that a multitude of possible scenarios exist [24].

Practical criteria for engineers to use in predicting the behaviors of dynamical systems are for the most part lacking when non-linearities are large. Moon and Holmes [15] have developed a heuristic criterion for the transition to chaos in systems modeled by Duffing's equation such as vibrations of a buckled beam. Although that criterion works reasonably well, the complexity of these systems has prevented a more general theory from being developed. A more rigorous criterion has been developed by Holmes [25] but is limited since it predicts regions which may be merely transiently chaotic. It also relies on small damping and forcing assumptions. At present one is largely limited to experiments and digital simulations to study the phenomena. Only the simplest systems are currently analytically tractable.

ACKNOWLEDGMENTS

The author would like to thank Professor Frank Moon at Cornell for suggesting these experiments and for providing the laboratory in which they were performed. Thanks are due also to Professor Philip Holmes at Cornell for several helpful comments.

REFERENCES

1. F. C. MOON and S. W. SHAW 1983 *International Journal of Nonlinear Mechanics* **18**, 465-477. Chaotic vibrations of a beam with nonlinear boundary condition.
2. S. W. SHAW and P. J. HOLMES 1983 *Journal of Sound and Vibration* **90**, 129-155. A periodically forced piecewise linear oscillator.
3. S. W. SHAW and P. J. HOLMES 1983 *Journal of Applied Mechanics* **50**, 849-857. A periodically forced impact oscillator with large dissipation.
4. S. W. SHAW and P. J. HOLMES 1983 *Physical Review Letters* **51**, 623-626. Periodically forced linear oscillator with impacts: chaos and long period motions.
5. H. G. DAVIES 1980 *Journal of Sound and Vibration* **68**, 479-487. Random vibration of a beam impacting stops.
6. L. A. WOOD and K. P. BYRNE 1981 *Journal of Sound and Vibration* **78**, 329-345. Analysis of a random repeated impact process.
7. L. A. WOOD and K. P. BYRNE 1981 *Journal of Sound and Vibration* **85**, 53-69. Experimental investigation of a random repeated impact process.
8. D. I. G. JONES and A. MUSZYNSKA 1979 *Nonlinear Vibrating Problems*, 153-178. Harmonic response of a damped two-degree of freedom system with gaps.
9. Y. A. MARIAMY, S. F. MASRI and J. C. ANDERSON 1980 *University of Southern California Report to U.S. Regulatory Commission, Report No. NUREG/CR-1318-RO*. Analytical and experimental studies of a beam with a geometric nonlinearity.
10. T. WATANABE 1978 *Journal of Mechanical Design* **100**, 487-491. Forced vibration of continuous system with nonlinear boundary conditions.
11. R. D. BLEVINS 1979 *Formulas for Natural Frequency and Mode Shapes*. New York: Van Nostrand and Reinhold Co.
12. W. T. THOMSON 1948 *Mechanical Vibrations*, New York: Prentice-Hall.
13. L. MEIROVITCH 1975 *Elements of Vibration Analysis*. New York: McGraw-Hill.
14. J. M. T. THOMPSON 1983 *Proceedings of the Royal Society London*, **A387**, 407-427. Complex dynamics of compliant off-shore structures.
15. F. C. MOON and P. J. HOLMES 1979 *Journal of Sound and Vibration* **65**, 275-296. A magnetoelastic strange attractor.
16. F. HENDRIKS 1983 *IBM Journal* **27**, 273-280. Bounce and chaotic motion in impact print hammers.
17. H. J. CONNERS 1982 *Nuclear Technology* **55**, 311-331. Flow induced vibration and wear of steam generator tubes.
18. G. H. LEAN 1971 *Transactions of the Royal Institution of Naval Architects* **113**, 387-399. Subharmonic motions of moored ships subjected to wave action.
19. S. W. SHAW 1983 *Ph.D. Dissertation*, Cornell University. *A periodically forced piecewise linear oscillator*.
20. P. S. LINSAY 1981 *Physical Review Letters* **47**, 1349-1352. Period doubling and chaotic behavior in a driven an-harmonic oscillator.
21. J. GUCKENHEIMER and P. HOLMES 1983 *Nonlinear Oscillations, Dynamical Systems and Bifurcations of Vector Fields*. New York: Springer-Verlag.
22. M. J. FEIGENBAUM 1980 *Los Alamos Science* **1**, 4-27. Universal behavior in nonlinear systems.
23. P. COLLET and J. P. ECKMANN 1980 *Iterated Maps on the Interval as Dynamical Systems*, *Progress in Physics*, No. 1. Boston: Birkhäuser.
24. P. J. HOLMES and D. C. WHITLEY 1984 *Philosophical Transactions of the Royal Society London* **A311**, 43-102. Bifurcations of one and two dimensional maps.
25. P. J. HOLMES 1979 *Philosophical Transactions of the Royal Society* **A292**, 419-448. A nonlinear oscillator with a strange attractor.